ANNUAL REVIEWS

Annual Review of Physical Chemistry

Characterization of Intermediate Oxidation States in CO_2 Activation

Leah G. Dodson,[1] Michael C. Thompson,[2] and J. Mathias Weber[2]

[1]JILA and NIST, University of Colorado, Boulder, Colorado 80309-0440, USA; email: leah@jila.colorado.edu

[2]JILA and Department of Chemistry and Biochemistry, University of Colorado, Boulder, Colorado 80309-0440, USA; email: michael.thompson@colorado.edu, weberjm@jila.colorado.edu

Annu. Rev. Phys. Chem. 2018. 69:231–52

First published as a Review in Advance on February 28, 2018

The *Annual Review of Physical Chemistry* is online at physchem.annualreviews.org

https://doi.org/10.1146/annurev-physchem-050317-021122

Keywords

carbon dioxide, formate, oxalate, carbonate, C–O activation, CO_2 reduction catalysis

Abstract

Redox chemistry during the activation of carbon dioxide involves changing the charge state in a CO_2 molecular unit. However, such changes are usually not well described by integer formal charges, and one can think of COO functional units as being in intermediate oxidation states. In this article, we discuss the properties of CO_2 and CO_2-based functional units in various charge states. Besides covering isolated CO_2 and its ions, we describe the CO_2-based ionic species formate, oxalate, and carbonate. Finally, we provide an overview of CO_2-based functional groups and ligands in clusters and metal–organic complexes.

1. INTRODUCTION

Chemical bonds are an efficient way to store energy, and chemical fuels are one of the most convenient sources of energy on demand through combustion or fuel cells. As a result, our civilization relies on the combustion of fuels, most of which are carbon-based and come from fossil deposits. Carbon dioxide (CO_2) is an important combustion product, and the continued use of fossil fuels increases atmospheric CO_2 concentrations. Although our planetary ecosystem as we know it relies on the presence of CO_2, current and projected concentrations of CO_2 will lead to a continued increase in global average temperatures and sea levels, with immense negative impact. Similarly, CO_2 is an important part of the acid–base chemistry in oceans and lakes, but its current high concentrations are leading to overacidification of the oceans. However, CO_2 could be harnessed as feedstock to produce chemical fuels on an industrial scale, using renewable energy sources to drive the conversion process. A carbon-neutral fuel cycle could be developed along these lines, taking advantage of the unsurpassed energy storage capacity of chemical bonds while also lessening the environmental impact of anthropogenic CO_2 emissions.

At first glance, CO_2 activation seems difficult and costly. It is a very stable molecule, with high bond dissociation energy [525.9 kJ mol^{-1} (1)] and ionization potential [13.777 eV (2)], and it has a negative electron affinity (see Section 2). Nonetheless, it can weakly donate electron density and has a remarkable ability to accept electron density where it occurs as a ligand or functional group, or as a part thereof. Reducing CO_2 provides the most convenient avenue to its chemical conversion. One-electron reduction of CO_2 is assumed to be the first step in most processes converting CO_2 to chemical fuels or to feedstock for other industrial use (3), although hydride transfer is considered to be an alternative with lower barriers (4). Reduction of CO_2 to more useful molecules requires multiple electrons and protons (3, 5), and different reduction processes can yield a number of products, such as carbon monoxide, formate, methanol, or oxalate (which is often invoked in the context of CO_2 fixation rather than conversion to fuel) (6). Carbon monoxide can be used to generate fuels by means of Fischer–Tropsch chemistry (7). Similarly, methanol, another possible product from CO_2 reduction, can be used as feedstock in methanol-to-olefin conversion to produce fuels (8).

Unfortunately, the reduction of CO_2 is energetically unfavorable for both free and solvated CO_2. Not only is this due to the obvious difference in free energy between CO_2 and final products, but there are also significant reaction barriers to be overcome during the conversion processes (3, 9). For CO_2 reduction to be economically viable, suitable catalysts need to be developed and adapted to the process used for the conversion (e.g., electrochemistry, photochemistry, or a combination thereof).

As in many other areas of chemistry, the simple concept of integer oxidation states does not hold particularly well when it comes to the description of the relevant reactions in CO_2 reduction, and intermediate oxidation states of CO_2 and related species must be considered to describe CO_2 conversion processes. There is an immense body of literature on the catalysis of CO_2 reduction, and this review is not intended to reiterate the many excellent recent reviews in this field (6, 10–14) or to be comprehensive. Instead, we focus on the characterization of CO_2 in intermediate oxidation states. In this context, we explore CO_2 as a molecule, but more importantly, CO_2 as a functional group or even as a subunit of a larger CO_2-based unit such as oxalate, characterizing molecular-level properties (for example, electron binding energies and vibrational signatures).

2. RELEVANT MOLECULAR PROPERTIES OF FREE CO_2 AND ITS IONS

To gain insight into possible avenues to characterize intermediate oxidation states, it is instructive to first look at the molecular properties of CO_2 in different charge states. Its electronic structure

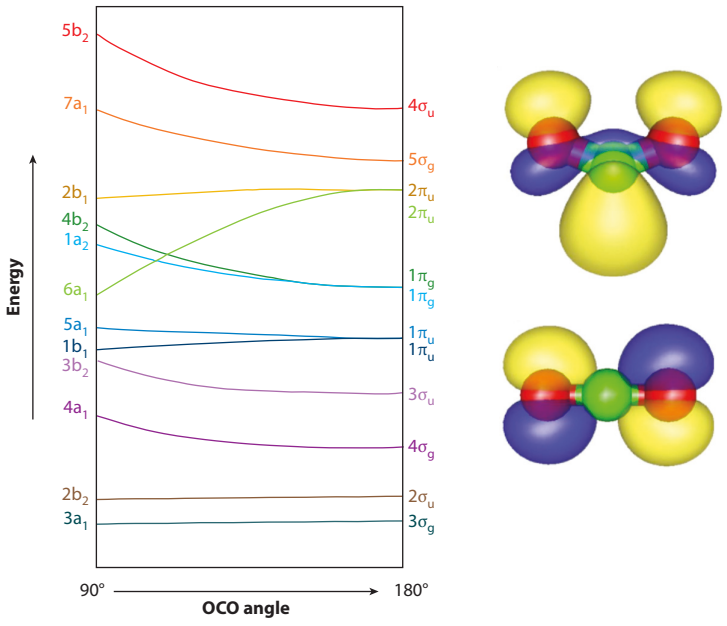

Figure 1

Walsh diagram (15, 16) of CO_2, with illustrations of the highest occupied molecular orbitals of the anion (*top*) and the neutral (*bottom*). Figure adapted from Reference 16 with permission (see also **http://www.informaworld.com**).

can be summarized in its Walsh diagram (15, 16) (see **Figure 1**), which is also a convenient tool to illustrate some of the properties of its ions.

In the ground state of neutral CO_2, the highest occupied molecular orbital (HOMO) is the fully occupied $1\pi_g$ orbital. An excess electron will be accommodated in the $2\pi_u$ orbital, which is stabilized by bending the molecule, leading to a deviation of the molecular symmetry from $D_{\infty h}$ to C_{2v}. The singly occupied molecular orbital (SOMO) in this radical anion in its electronic ground state is of a_1 symmetry, with an OCO angle calculated to be 138° (17), and it can be described as pseudo-antibonding (18). At the same time, the bonding $1\pi_g$ orbital transforms into a_2 and b_2 orbitals that have been characterized as largely nonbonding (18). Consistent with the pseudo-antibonding nature of the HOMO of CO_2^-, its C–O bond length (124 pm) is greater than that of neutral CO_2 (117 pm) (17).

The adiabatic electron affinity of CO_2 is not precisely known but is clearly negative. It is estimated to be −0.6 eV (19); in other words, the free CO_2^- radical anion is unstable against electron emission and is better described as a temporary negative ion state or electron scattering resonance. Quantum chemistry calculations recover this fact (17, 20). However, the vertical electron detachment energy (VDE) of CO_2^- is about 1.4 eV (21), indicating that CO_2^- is metastable, and it has been observed in mass spectrometry experiments, with measured lifetimes up to milliseconds (22–24). In addition, the radical anion can be stabilized by interaction with a matrix [e.g., a rare gas matrix (25–27)] or by solvation. The solvated CO_2^- radical anion has been observed in bulk solutions (28–30) as well as in $(CO_2)_n^-$ ($n = 6$–13) cluster ions (31–33).

Since the SOMO in CO_2^- is (pseudo-)antibonding, its antisymmetric CO stretching vibrational frequency shifts to the red compared to neutral CO_2, from 2,349 cm^{-1} to about 1,660 cm^{-1} (26, 34). At the same time, the bending frequency shifts to the blue, from 667 cm^{-1} to about 714 cm^{-1}

OSCILLATOR COUPLING AND CO STRETCHING MODES IN CO_2

The changes in the symmetric (ν_s) and antisymmetric (ν_{as}) stretching frequencies upon addition of an excess electron are based on two effects: (*a*) changes in the mechanical coupling of the two CO oscillators by bending the molecule and (*b*) weakening of the CO bonds. By itself, the former diminishes the splitting between ν_s and ν_{as}, shifting ν_{as} to the red and ν_s to the blue, while the latter leads to a redshift for both modes. For ν_{as}, both effects add, exacerbating the overall shift. For ν_s, the two effects partially cancel each other. Similar effects are observed for $-COO^-$ groups, where a divalent metal ion forces a less obtuse OCO bond angle than would be found in an uncoordinated $-COO^-$ group (35). Simple calculations (36) comparing the shifts of ν_{as} and ν_s from CO_2 to CO_2^- qualitatively show the effect of weakening the CO bonds separately. For a CO_2 molecule in which the CO oscillators are mechanically decoupled by a very heavy central carbon atom (e.g., 10^4 u), both ν_{as} and ν_s start at similar frequencies in the neutral molecule, and both shift to the red by similar amounts upon electron attachment. This is in contrast to regular CO_2, as described above.

(26, 34). Also, the bent CO_2^- geometry leads to a decrease in the kinetic coupling of the CO oscillators; the combination of the decreased coupling and the (pseudo-)antibonding SOMO results in a strong redshift of the antisymmetric CO stretching mode but only a weak effect on the symmetric stretching mode, although the latter becomes infrared-allowed in the anion (see the sidebar titled Oscillator Coupling and CO Stretching Modes in CO_2). As a consequence of the changes in the vibrational spectrum, the pronounced Fermi resonance between the fundamental of the symmetric CO stretching mode and the bending mode overtone in neutral CO_2 does not exist in CO_2^-. The shifts of the vibrational modes, particularly the redshift of the CO stretching vibrational modes, offer an experimental way to probe the charge density on a CO_2 molecule or even a COO functional group in an R–COO molecule, as we discuss in Section 5.

The electronic structures of CO_2 and CO_2-containing functional groups also provide an avenue for experimental characterization via, for example, photoelectron spectroscopy. The electron binding energy is a marker for the chemical identity of CO_2-based species. While the first electronic excited state of neutral CO_2 is in the deep ultraviolet (UV), the radical anion has its lowest excited state in the near UV (37–40). The electronic absorption band of CO_2^- at about 235 nm has been used for resonance Raman spectroscopy (30). However, CO_2^- can dissociate upon excitation (38–40), and its rather broad absorption bands limit the use of CO_2^- electronic excited states for characterization of CO_2^- and related systems. In addition, the radical anion can lose its excess electron by detachment or charge transfer to a solvent (30).

The CO_2^+ radical cation, i.e., the result of CO_2 oxidation, is a stable ion, in contrast to the radical anion. It has an appearance energy of 13.777 eV (2), highlighting the exceptional stability of the closed-shell neutral CO_2 molecule against ionization. The cation is a linear molecule, and the $1\pi_g$ orbital is not completely filled. Since this orbital is bonding, the vacancy causes a weakening of the CO bonds compared to the neutral molecule and a concomitant redshift of the CO stretching frequencies and of the bending frequency (41). The antisymmetric stretching frequency is more strongly shifted (to about 1,423 cm^{-1}) than the symmetric stretching mode (to about 1,242 cm^{-1}). This anomalously strong shift of the antisymmetric stretching mode has been explained by vibronic interaction between the $\tilde{X}^2\Pi_g$ and $\tilde{A}^2\Pi_u$ states through this vibrational mode (see, e.g., 42 and references therein). Because of the high ionization potential of neutral CO_2, the cation is not often observed in the condensed phase, since it is likely to abstract an electron from most solvent molecules, as data on cationic clusters containing CO_2 show (43).

3. STRUCTURAL AND ELECTRONIC PROPERTIES OF REDUCED DIMERIC CO_2: THE $C_2O_4^-$ ION

The $C_2O_4^-$ ion is particularly interesting for the characterization of CO_2 at intermediate oxidation states because, in a zeroth-order picture, the singly charged anions represent CO_2 moieties at oxidation states of −0.5. In contrast to the CO_2^- monomer anion, the dimer anion is a stable species (21, 31, 32, 44). The CO_2 dimer anion, $C_2O_4^-$, has D_{2d} symmetry (45), and the charge in the dimer is symmetrically distributed over two bent CO_2 units (see **Figure 2**). The dimer anion structure can be qualitatively understood as a charge-resonance structure mixed between $CO_2^- \cdot CO_2$ and $CO_2 \cdot CO_2^-$ charge-localized states, giving rise to an intermediate oxidation state of −0.5 for each CO_2 subunit. In line with this picture, the HOMO of the dimer anion can be viewed as a linear combination of the antibonding $6a_1$ orbitals of the two bent CO_2 units constituting the dimer (see **Figure 2**), forming a C–C σ-bond. Coulomb repulsion between the oxygen atoms in the dimer anion stabilizes the D_{2d} structure. The vertical detachment energy of $C_2O_4^-$ is 2.79 eV (31), and the adiabatic electron affinity can be estimated to be about 1.7 eV, but photoelectron spectroscopy experiments have not provided a precise value because of the highly congested photoelectron spectrum (21, 31, 32, 44), and the actual value remains unknown. Interestingly, coupled-cluster calculations at the CCSD(T) level (45) predict a negative adiabatic electron affinity. Calculations give a C–C bond length of 189.8 pm and a C–O bond length of

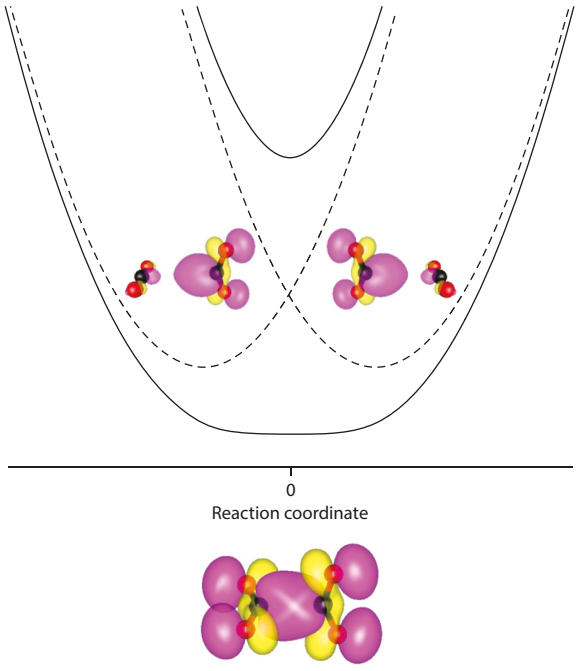

Figure 2

Schematic potential energy diagram, structure, and highest occupied molecular orbital of the $C_2O_4^-$ ion. The dashed lines represent model diabatic states with the excess charge localized on one of the CO_2 units (see schematic structures, *top*), while the solid lines show adiabatic states derived by mixing the diabatic states as a strongly coupled two-level system, with the bottom structure depicting the ground state of $C_2O_4^-$. The reaction coordinate corresponds to the localization of the charge on one versus the other CO_2 monomer and can be parametrized using the difference in the OCO bond angles of the two CO_2 units and the C–C distance (see also 33).

122 pm; the C–O bond length is slightly greater than that in a neutral CO_2 dimer (117 pm). The greater C–O bond length reflects the population of an orbital that is net-antibonding for the C–O interaction, similar to the CO_2^- monomer anion (124 pm) (17).

The $C_2O_4^-$ anion has five infrared active normal modes, and some have been observed in rare gas matrix isolation experiments (26, 27, 46) and in $(CO_2)_n^-$ clusters (33, 47, 48), where they depend on cluster size. The most intense signature is due to a (degenerate) antisymmetric stretching vibration of *e* symmetry in the range 1,852–1,900 cm^{-1}, depending on the matrix. This feature consists of at least four partially resolved components, with the two most prominent peaks at about 1,865 cm^{-1} and 1,890 cm^{-1}. Unfortunately, the individual components of this feature have never been rigorously assigned by anharmonic calculations. The symmetric stretching motion of the two CO_2 units gives rise to a strong b_2 band that appears at 1,180–1,190 cm^{-1}. The similarly strong b_2 band corresponding to the out-of-phase combination of the bending vibrations of the two CO_2 units has been found at 679.9 cm^{-1} (26) in a Ne matrix and at 674 cm^{-1} in $(CO_2)_n^-$ clusters (48). Two degenerate *e* symmetry wagging modes are predicted at lower frequencies, but have not been observed experimentally.

The $C_2O_4^-$ ion has been observed as a core ion in neat CO_2 cluster anions $(CO_2)_n^-$ in the size regimes $n \leq 6$ and $n = 14$–17, whereas the core ion for clusters between those size regimes is a CO_2^- anion (31–33, 44). This curious behavior reflects a subtle balance between intrinsic electronic stability (which favors the $C_2O_4^-$ ion at the smallest cluster sizes) and the size-dependent solvation energy that a given core ion in a $(CO_2)_n^-$ cluster gains, which cannot be described using dielectric continuum models for the solvent. Unlike solvation by CO_2 molecules, hydration of $C_2O_4^-$ leads to a localization of the excess electron on a single CO_2 moiety for as few as two water molecules (38, 49, 50). Solvation by methanol also shows preferential localization on a single CO_2 unit (51). The response of $C_2O_4^-$ to solvation reflects the delocalized nature of the dimer anion and its high inherent polarizability.

4. CO_2-BASED CONJUGATE BASE ANIONS: FORMATE, OXALATE, AND CARBONATE

4.1. Formate (HCO_2^-)

From the viewpoint of intermediate oxidation states of CO_2, in the formate anion (HCO_2^-), the CO_2 unit is bent, bearing significant negative charge (52), with the hydrogen atom binding to the carbon atom, resulting in overall C_{2v} symmetry. Negative ion photoelectron spectroscopy experiments determined the adiabatic electron binding energy to be 3.498 ± 0.015 eV (53). The OCO bond angle for gas-phase HCO_2^- was determined in CCSD(T) calculations to be 130°, with C–O bond lengths of 125–126 pm (54). The symmetric and antisymmetric C–O stretching modes appear at $\nu_s = 1{,}314$ and $\nu_{as} = 1{,}622$ cm^{-1}, respectively, measured for argon-tagged gas-phase HCO_2^- (52, 55); these values are within 10 cm^{-1} of the observed values for matrix-isolated HCO_2^- (56). These modes shift slightly more in water, with a predicted change in OCO angle of less than one degree, and observed vibrations lie within 30 cm^{-1} of solution values (see 55 and references therein). Gerardi et al. (55) observed the $\nu_s + \nu_{as}$ combination band at 2,928 cm^{-1} in the gas phase.

The C–H stretching mode in HCO_2^- is highly anharmonic, with a fundamental energy that is anomalously low in the gas phase and in rare gas matrices, with a calculated C–H bond distance of 113 pm and a measured gas-phase vibration at 2,449 cm^{-1}. Upon solvation with just one water molecule, which binds to the COO^- group, ν_{CH} shifts by more than 100 cm^{-1} to the blue, bringing this mode much closer to the bulk value. In both aqueous and polycrystalline $NaHCO_2$, ν_{CH} is in the range 2,800–2,830 cm^{-1} (57, 58).

Krekeler et al. (54) and Gerardi et al. (55) both theoretically considered the process of breaking the CH bond. In the intact HCO_2^-, the excess electron is first localized on the CO_2 moiety, but as the CH bond is elongated, a rapid transition occurs in the range $r_{CH} = 150$–250 pm, resulting in localization of the electron on the H atom and creating $CO_2 + H^-$ as products. The energy threshold for this process is predicted to be 216 kJ mol^{-1}.

4.2. Oxalate ($[C_2O_4]^{2-}$) and Hydrogen Oxalate ($[C_2O_4H]^-$)

The oxalate ion, $[C_2O_4]^{2-}$, is a product of CO_2 reduction under aprotic conditions (59), and it also appears as a ligand in metal–CO_2 cluster ions (see Section 5), making it relevant for the present discussion. It can be thought of as two CO_2^- monomer ions with an overall charge of −2 e symmetrically distributed between the two fully reduced CO_2 subunits. Not surprisingly, the bare singlet dianion species $[C_2O_4]^{2-}$ has negative vertical and adiabatic detachment energies and is unstable with respect to autodetachment (60, 61). For the (hypothetical) free dianion, both the staggered structure with D_{2d} symmetry and the planar structure with D_{2h} symmetry have been evaluated computationally, with the D_{2d} form being consistently lower in energy (see, e.g., 61–65). Rotation about the long C–C single bond between the two CO_2 units in the dimer (there is essentially no C–C π-bonding) connects the two structures, with the D_{2h} energy lying 18.0 kJ mol^{-1} above the D_{2d} energy (65). Because of Coulomb repulsion, the C–C single bond between the two CO_2 units is quite long; it is typically predicted to be about 155 pm for the structure with D_{2d} symmetry and about 106 pm in the D_{2h} structure.

Although the free oxalate dianion is unstable with respect to electron loss, it is stabilized by solvation. Hydration of $[C_2O_4]^{2-}$ produces stable $[C_2O_4]^{2-} \cdot (H_2O)_n$ clusters starting at $n = 3$ (61, 66), and the vertical and adiabatic electron binding energies increase systematically with increasing solvation up to cluster sizes of $n = 40$. Extrapolation from cluster values to bulk (67) predicts a VDE of 6.92 eV, close to the experimental value in bulk aqueous solution, VDE = 7.32 eV (68).

For small clusters, the hydrated $[C_2O_4]^{2-}$ ion has a reduced O–C–C–O torsion angle compared to the structure with D_{2d} symmetry, but it remains nonplanar. The first four water molecules interact strongly with the $[C_2O_4]^{2-}$ ion through two hydrogen bonds each, lacking any water–water interactions; with additional water molecules, however, a water network begins to form around the ion. In bulk solution, infrared and Raman spectra of aqueous oxalate ion showed that the $[C_2O_4]^{2-}$ ion takes a D_{2d} form (69–71). However, thermal fluctuations in aqueous solutions are likely to lead to sampling of torsion angles of up to ±30° about the global minimum torsion angle at 90° (65).

The vibrational modes of aqueous $[C_2O_4]^{2-}$ have been assigned, after some debate in the literature, using isotopic labeling experiments and computational analysis (see 70–72 and references therein). Infrared signatures assigned to the D_{2d} symmetric stretching modes are observed at 905 cm^{-1} and 1,490 cm^{-1}, and antisymmetric stretching modes appear at 1,310 cm^{-1} and 1,575 cm^{-1}, respectively. Compared to CO_2^-, the calculated C–O bond length increases from 123 pm to 128 pm, and the O–C–O bond angles decrease from 138° to 126° (27, 65).

Addition of a proton to oxalate results in the formation of hydrogen oxalate, $[C_2O_4H]^-$, a singly charged ion that can be thought of as either protonated oxalate or deprotonated oxalic acid, which is stable with respect to autodetachment (65, 73). In the gas phase, the proton binds to one of the four oxygen atoms and forms an intramolecular hydrogen bond to an oxygen atom in the CO_2^- group, resulting in a planar structure. The presence of the proton causes significant decoupling of the four CO stretching oscillators. Vibrational spectroscopy of cryogenically cooled $[C_2O_4H]^-$ monoanions (73) shows the free carbonyl stretch (the C=O stretch on the COOH side of the ion) at 1,766 cm^{-1} and the symmetric and antisymmetric C–O stretching modes of the COO^- group at about 1,320 cm^{-1} and 1,700 cm^{-1}, respectively. The antisymmetric stretching frequency

of the COO^- moiety in the hydrogen oxalate anion falls between the values of the CO_2^- anion and neutral free CO_2 (2,349 cm^{-1}) (34), which is consistent with the idea that the COO^- group in hydrogen oxalate is in an intermediate oxidation state, i.e., not fully reduced (16).

4.3. Carbonate (CO_3^{2-}) and Bicarbonate (HCO_3^-)

In the context of CO_2 at intermediate oxidation states, carbonate and related species fill an interesting role. It is not straightforward to talk about carbonate as CO_2 in a reduced or oxidized form, since it is a product of acid–base chemistry rather than redox chemistry. It is instructive, however, to consider a hypothetical, free CO_3^{2-} dianion in its D_{3h} structure, viewing it (somewhat artificially) as a CO_2 moiety with an added oxygen atom, where the formal charge on each oxygen atom is −2/3 e. From this point of view, the CO_2 moiety is bent and negatively charged, and many of its properties (particularly its vibrational behavior) are close to those of a negatively charged, CO_2-based functional group or ion.

The near-synonymous use of CO_2 and carbonate in (aqueous) solution is based on the set of equilibria

$$CO_2 + H_2O \leftrightarrow H_2CO_3 \leftrightarrow HCO_3^- + H^+ \leftrightarrow CO_3^{2-} + 2H^+.$$

The delicate balance of these equilibria has a significant impact in a range of fields, including ocean acidification, carbonate dissolution in mineralogy and geology, and regulation of blood pH (74, 75). When CO_2 is dissolved in water, the equilibrium between carbonic acid and bicarbonate so heavily favors the conjugate base (and the reaction of CO_2 with water is so slow) that less than 1% of the solution exists as H_2CO_3. The balance is complicated by factors such as solvation-catalyzed $CO_2 + H_2O$ reactions, the equilibrium between CO_2(g) and CO_2(aq), and autoprotolysis (76).

The carbonate dianion, CO_3^{2-}, is predicted to have D_{3h} symmetry in the gas phase, although it has never been isolated and is unstable against electron loss (77–79). In aqueous solution, infrared and Raman spectra demonstrate that the D_{3h} structure is never present, even in very dilute solutions (76, 80–86). Notably, the nominally infrared-forbidden symmetric C–O stretching mode at about 1,064 cm^{-1} appears strongly in both infrared and Raman spectra. Similarly, the out-of-plane deformation mode, ν_2, appears in both infrared and Raman spectra near 880 cm^{-1}, even though it is nominally Raman-forbidden (assuming D_{3h} symmetry). Asymmetric solvation and ion pairing have been implicated in breaking the symmetry of CO_3^{2-} in aqueous solution. The degeneracy of the antisymmetric C–O stretching mode is lifted, giving rise to two modes around 1,400 cm^{-1}, split by 80–370 cm^{-1} (87). Their splitting depends on whether the interaction with the environment (e.g., ions or surfaces) is predominantly monodentate or bidentate (81, 87–89).

Gas-phase bicarbonate, HCO_3^-, is expected to have C_s (planar) symmetry, while it has C_1 symmetry in dilute aqueous solutions, with the hydrogen atom protruding from the σ_h plane of the CO_3 scaffold (76, 86). Notable features include the C–O symmetric and antisymmetric stretching modes at 1,364 cm^{-1} and 1,634 cm^{-1}, respectively. The most intense band is the CO stretching mode involving the hydroxyl group, which appears at 1,014 cm^{-1} and can be used in conjunction with nearby spectral features from other chemical species (CO_3^{2-} or H_2O network vibrations) to quantify bicarbonate concentrations in solution (76, 90). The OH stretching mode has been assigned in experimental spectra at 2,615 cm^{-1}, but this value disagrees with harmonic approximation calculations by ∼1,000 cm^{-1}, suggesting that it is highly anharmonic (86).

In order to assess the microsolvation environment of HCO_3^- in more detail, Garand et al. (91) probed small clusters of $HCO_3^- \cdot (H_2O)_n$ ($n = 1$–10) using infrared multiphoton photodissociation spectroscopy. Their work shows that water preferentially solvates the side of the HCO_3^- ion opposite from the OH group, in which the negative charge is shared between the two free oxygen

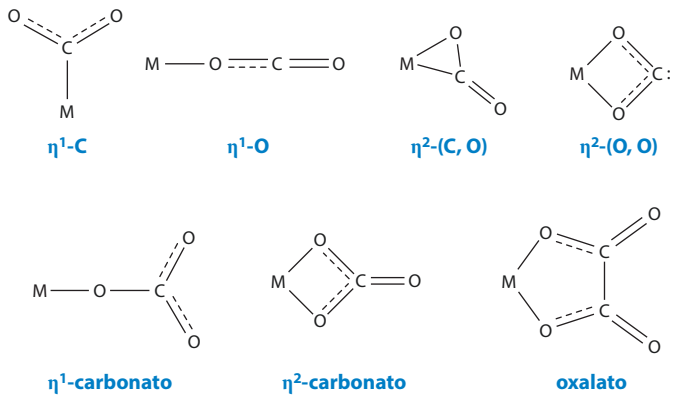

Figure 3

Structural motifs of metal–CO_2 interactions.

atoms, and which is reminiscent of a formate functional group. Solvation in this position strengthens the alcoholic C–O bond while weakening the others. The symmetric and antisymmetric CO stretching vibrational modes were found at about 1,300–1,350 cm^{-1} and 1,650–1,700 cm^{-1}, respectively. Unfortunately, Garand et al. did not address the OH stretching mode, and a better assessment of its anharmonicity is still needed.

5. CO_2-BASED LIGANDS

The interaction of CO_2 with metal surfaces, metal atoms, and metal centers in metal–organic complexes is of great interest in the context of CO_2 reduction catalysis. The interaction of CO_2 with metal atoms has been investigated in solutions and on surfaces, as well as by studying matrix-isolated species and mass-selected cluster ions.

There are several binding motifs of CO_2 to single metal centers. In the limiting case of a single CO_2 ligand binding to a metal atom, four binding motifs are currently known. In line with the nomenclature of metal–organic chemistry, they can be abbreviated as η^1-C, η^1-O, η^2-(C,O), and η^2-(O,O), where superscripts denote the number of bonds between the metal atom and the CO_2 ligand and chemical element symbols describe the atoms directly interacting with the metal (see **Figure 3**). Carbonate and oxalate represent more complicated ligands, with more than just a CO_2 subunit. There are additional binding scenarios for complexes with multiple metal atoms (92, 93), but we restrict our discussion to complexes with single metal centers.

One characterization method that is common to most chemical environments is vibrational spectroscopy, and much of our discussion in this section is therefore concerned with the vibrational spectra of CO_2 and related species bound as ligands to metals. **Figure 4** summarizes the spectral regions of interest for the CO stretching vibrations of these CO_2-based ligands (see the discussion below).

Cationic metal–CO_2 complexes have received much attention over the past decades because of interest both in the reactivity of CO_2 with metal surfaces and in the bonding of closed-shell ligand systems to a metal center. Gas-phase experiments, particularly work on mass-selected ions, can give detailed insight into fundamental aspects of metal–CO_2 interactions. Cationic metal–CO_2 complexes and clusters are largely dominated by electrostatic interactions. The thermochemistry of metal–CO_2 interactions in such systems has been examined by the Armentrout and Schwarz groups for a number of metal species (see, e.g., 94, 95 and references therein), and their

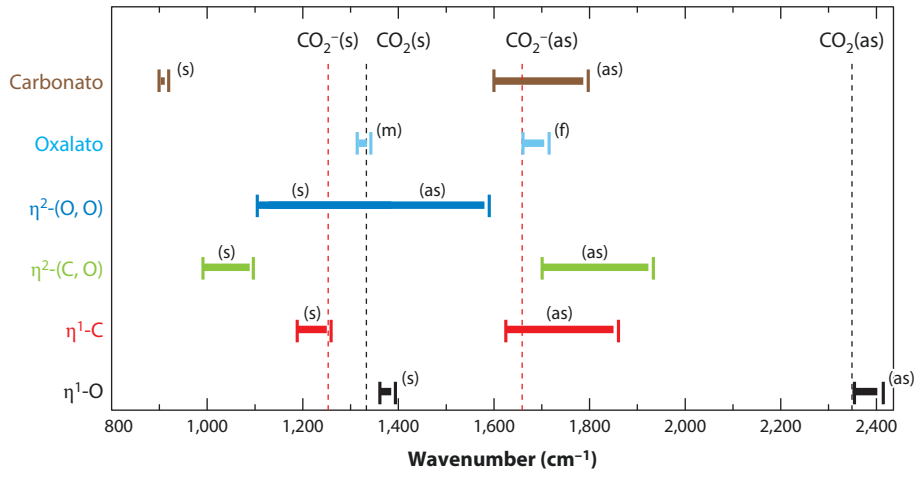

Figure 4

Range of wavenumbers for signatures in metal–ligand complexes involving CO_2-based ligands discussed here (for nomenclature, see **Figure 3**). Symmetric (s) and antisymmetric (as) characters for the vibrational modes are indicated, except for the oxalate core ion, where the labels of free (f) and metal-bound (m) are more appropriate. Dashed vertical lines correspond to signatures of neutral (*black*) and anionic (*red*) CO_2. The line representing the symmetric stretching mode in neutral CO_2 shows an average of the two components of its Fermi resonance with the bending overtone.

metal–CO_2 bond strengths typically measure a few hundred millielectronvolts. The Duncan (48, 96–102) and Mackenzie (103) groups have examined a number of such systems using infrared photodissociation spectroscopy, including V^+, Si^+, Ni^+, Mg^+, Fe^+, Al^+, Ca^+, Co^+, Rh^+, and Ir^+. In most $[M(CO_2)_n]^+$ cluster cations, the CO_2 molecule interacts end-on with the metal ion through one of its oxygen atoms (η^1-O), dominated by charge-quadrupole interactions and a linear M^+–O=C=O structure. Typically, M–O distances are calculated to be about 210–230 pm, depending on the metal and the size of the cluster. The CO_2 molecules can be largely characterized as solvent molecules, solvating a metal cation, and each solvent molecule in the first solvation shell has roughly the same type of interaction with the metal center. Spectroscopically, these metal-solvating CO_2 complexes exhibit antisymmetric CO stretching signatures that are typically blueshifted by 20–30 cm^{-1} compared to free CO_2. Duncan and coworkers (98) explained this blueshift with the assumption that the CO stretching motion involving the oxygen atom near the metal will encounter an additional repulsive force close to the outer turning point of the vibration as it comes closer to the metal atom. A similar interaction motif can be at play in metal–organic complexes with bulky organic ligands, as has been shown in a recent example in $[Ru(bpy)(tpy)(CO_2)]^{2+}$ (bpy = 2,2′-bipyridine; tpy = terpyridine), where the CO_2 ligand binds to the Ru^{II} metal center in the η^1-O binding motif (104), according to density functional theory. It is important to note that the CO_2 ligand in this case was added in the gas phase, in contrast to other metal–organic complexes synthesized with CO_2 ligands in solution, where other interaction motifs have been observed (see below). In all these cases, the CO_2 molecules in direct contact with the metal center are calculated to be slightly positively charged, with the CO bond on the metal side elongated by about 1% and the other CO bond shortened by roughly the same amount.

If the combination of the overall charge in a complex or cluster and the oxidation state of the metal favors electron transfer to one or more CO_2 ligands, the resulting metal–CO_2 interactions can differ significantly from the simple electrostatic η^1-O motif. Vanadium–CO_2 cluster cations

present a striking example. Whereas one might expect these clusters to behave similarly to other $[M(CO_2)_n]^+$ cluster ions, they show vibrational signatures indicating charge transfer to the surrounding CO_2 molecules, resulting in the formation of a CO_2 dimer anion and a V^{2+} ion (48). Specifically, a band at 1,140 cm^{-1} was interpreted as the b_2 band of the CO_2 dimer anion, shifted by about 50 cm^{-1} toward lower wavenumbers compared to $(CO_2)_n^-$ clusters. An additional band at 1,800 cm^{-1} was assigned to be the remnant of a group of bands associated with the $C_2O_4^-$ ion at 1,865 cm^{-1} and 1,890 cm^{-1} (see also Section 3). This intracluster reaction is observed only for larger clusters ($n \geq 7$), indicating that it is driven by solvation. Together with the emergence of the putative CO_2 dimer anion signature at 1,800 cm^{-1}, the antisymmetric stretching modes for the solvent molecules in the first shell of the vanadium ion are more strongly shifted to higher wavenumbers (about 2,400 cm^{-1}) compared to those associated with first-shell solvent molecules at smaller cluster sizes (2,380 cm^{-1}). These blueshifts constitute additional evidence for the intracluster reaction, since they point toward the presence of a more highly charged metal atom. It is interesting to note that similar blueshifted signatures were found for large $[Ni(CO_2)_n]^+$ and $[Si(CO_2)_n]^+$ clusters (96, 97). This observation suggests that intracluster reactions may occur similarly for those ions, but the lower wavenumber regions that would indicate the presence of CO_2 dimer anion products were not studied for these clusters.

Metal–CO_2 interaction in the presence of an excess electron generally leads to the reduction of one or more CO_2 ligands, as has been observed in metal–CO_2 cluster anions, $[M(CO_2)_n]^-$. These clusters can be seen as simplified model systems for the interaction of atomically rough metal surfaces with strongly undercoordinated metal atoms. It is widely believed that on supported nanoparticles or atomically rough surfaces used as cathodes in electrochemical CO_2 reduction, corner and edge sites are the main catalytically active structural moieties (105–108). Such sites may promote CO_2 reduction via a number of different motifs. Specifically, the electrophilic carbon atom is attracted to the high charge densities at such undercoordinated sites. Depending on the metal and on the cluster size, metal–CO_2 cluster anions can exhibit an astonishing degree of complexity, with many different possible core ion isomers.

Anionic clusters of CO_2 with coinage metal and bismuth atoms exhibit the metalloformate motif (η^1-C), with a single bond between the metal and the electrophilic C atom of a CO_2 molecule. Ab initio calculations show that there is significant overlap between an occupied s-orbital (in the case of Ag, Au, Cu) (109–111) or an occupied p-orbital (in the case of Bi) (112) and the empty π^* orbital of the CO_2 ligand. This results in a partial reduction of the CO_2 ligand, as the excess electron density is shared between the metal and the CO_2 unit. The presence of excess electron density in the π^* orbital of the COO^- moiety is encoded in the CO stretching modes of the $[M\text{-}COO]^-$ complex, as the CO bond strength decreases compared to neutral CO_2. As a consequence, the average of the frequencies of the symmetric and antisymmetric CO stretching modes shifts to the red by several hundred cm^{-1} compared to neutral CO_2 (109–112). The redshift can be quite large, comparable with the difference for these modes between CO_2^- and CO_2 (see Section 2).

The excess electron in metalloformate complexes is highly polarizable. As solvation in these complexes occurs preferentially at the COO^- functional group, the presence of solvent molecules polarizes the excess charge toward the COO^- moiety, and the extent of reduction depends on the level of solvation of the metalloformate anion. As a result, the antisymmetric CO stretching mode of the metalloformates generally shifts to the red with increasing solvation on the COO^- group (109–112). At the same time, an increase in excess electron density on the carboxylic group results in the OCO bond angle becoming more acute. This geometry change leads to a decrease in kinetic coupling of the two CO oscillators that constitute the COO^- group. As a consequence, the symmetric CO stretching mode shifts to the blue with increasing solvation, although the average of the symmetric and antisymmetric CO stretching modes continues to shift to the red

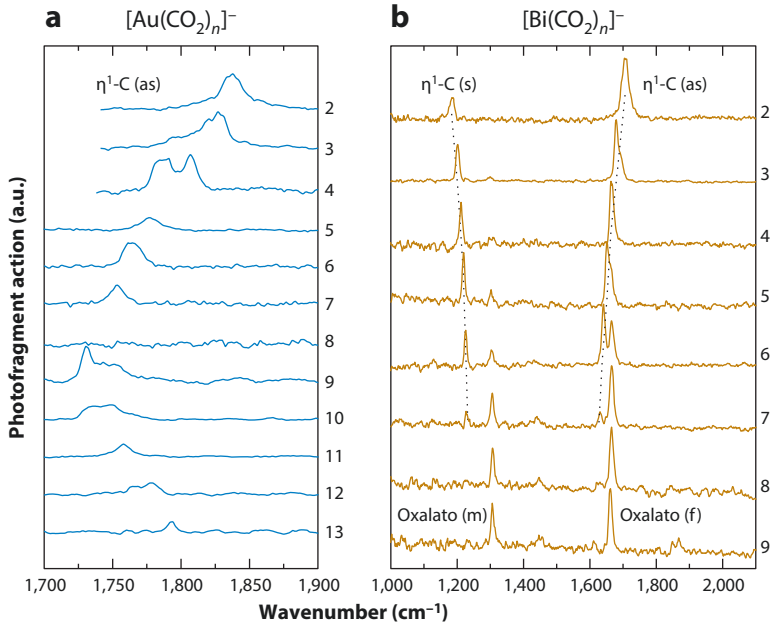

Figure 5

Infrared spectra of $[M(CO_2)_n]^-$ cluster anions, where the numbers at the right of each panel denote the cluster size. (*a*) M = Au (106); all signatures are due to the antisymmetric CO stretching mode of the $AuCOO^-$ core ion of the clusters. (*b*) M = Bi (109); signatures labeled η^1-C (s) and η^1-C (as) are assigned to symmetric and antisymmetric CO stretching modes of $BiCOO^-$ core ions, respectively, and marked with dotted lines; features marked oxalato (f) and oxalato (m) are the free and metal-bound CO stretching features of $[Bi^+(C_2O_4)^{2-}]$ core ions, respectively.

with increasing charge on the carboxylic group, reflecting the expected weakening of the CO bonds (112). In the limit of a very weak interaction of CO_2 with an atomic anion, a remnant of the η^1-C motif has also been observed in clusters of CO_2 with the heavier halides (I, Br, Cl) (113–116). In these cases, only little charge transfer to the CO_2 moiety occurs, and the deviation of the OCO bond angle from a linear configuration is less than 20°. In qualitative terms, the antisymmetric stretching vibration of a CO_2 ligand bound in an η^1-C motif will shift to the red with increasing charge on the COO^- functional group, and its position is a sensitive probe for the charge distribution (see the sidebar titled Oscillator Coupling and CO Stretching Modes in CO_2). Auroformate [$AuCOO^-$ (109)] and bismuthoformate [$BiCOO^-$ (112)] are particularly clear examples of this behavior (see **Figure 5**). There is a pseudolinear correlation between the charge on the COO^- group and the position of the antisymmetric stretch that is common to the coinage metals (Au, Ag, Cu) in the η^1-C motif. This curve even extrapolates to the CO_2^- anion in the limit of complete one-electron reduction (16). However, this simple connection does not hold universally for other systems, e.g., for $BiCOO^-$ (112).

The η^1-C binding motif has also been invoked in a variety of metal–organic coordination complexes where one coordination position is occupied by a CO_2 ligand but where bulky ligands restrict access to the metal center (92, 93). Specifically, some metal–CO_2 complexes with Rh and Ir centers have been characterized that feature this binding motif, with symmetric and antisymmetric stretching modes assigned to infrared absorptions at 1,210 cm^{-1} and 1,610 cm^{-1} for the Rh complex (117) and at 1,230 cm^{-1} and 1,550 cm^{-1} for the Ir complex (118), the latter suggesting significant

charge transfer to the CO_2 ligand. Tanaka & Ooyama identified the η^1-C binding motif for CO_2 in a ruthenium bipyridine-based complex via X-ray diffractometry (119). The η^1-C binding motif has also been proposed as the binding motif for CO_2 in a number of proposed catalytic mechanisms for polypyridine-based CO_2 reduction catalysts with Ru, Mn, Re, Fe, and Co centers (see, e.g., 119–121 and references therein). Other molecular CO_2 reduction catalysts in which the η^1-C motif has been invoked consist of macrocycles, such as porphyrins or cyclam (10, 122–125) with metal centers (particularly Fe, Ni and Co). However, while this binding motif has been frequently inferred, its presence often remains an unconfirmed hypothesis.

Another interaction motif observed in the interaction of CO_2 with transition metals is the η^2-(C,O) motif, where the CO_2 ligand forms both metal–oxygen and metal–carbon bonds. In this binding motif, a significant amount of charge (up to -1 e) is transferred into the π^* orbital of the CO_2 ligand, resulting in the complexes having a cationic or neutral metal center and an almost fully reduced CO_2 ligand. The vibrational spectra of gas-phase metal–CO_2 anionic clusters, $[M(CO_2)_n]^-$, with M = Fe, Co, Ni, or Cu, show evidence for this binding motif (111, 126–128), with characteristic vibrational features at 1,650–1,750 cm^{-1}. When two CO_2 ligands bind to the same metal center in this configuration, the metal exists as a monocation. The infrared signatures of these butterfly complexes can be distinguished from complexes with a single CO_2 ligand by the appearance of strongly coupled in-phase and out-of-phase combinations of symmetric and antisymmetric CO stretches in the individual ligands, which appear around 1,100 cm^{-1} and 1,700 cm^{-1}, respectively.

Vibrational spectra of gas-phase metal-oxide CO_2 anionic clusters, $[NiO(CO_2)_n]^-$ and $[CoO(CO_2)_n]^-$ (129), also exhibit the η^2-(C,O) motif, with similar vibrational frequencies. Calculations by the Jarrold group to interpret their photoelectron spectroscopy work suggest the formation of an η^2-(C,O) connected CO_2 molecule as the transition state in the reaction of CO_2 with $W_xO_y^-$ cluster anions (130, 131). The group concluded that reaction of tungsten oxide anions with CO_2 results in the oxidation of the cluster and the formation of unbound CO molecules.

While quantum chemical calculations clearly recover η^2-(C,O) connectivity for many of the metal–CO_2 cluster anion systems discussed above, the literature for metal–cyclam and other metal–organic complexes in CO_2 reduction catalysis has been ambiguous on whether the metal–CO_2 interaction follows the η^1-C or the η^2-(C,O) motif (125, 132–135). Using isotopic substitution of the CO_2 ligand in Ni(I)cyclam derivatives, Johnson and coworkers (136) have observed evidence for η^2-(C,O) binding. Overall, the η^2-(C,O) motif is quite common in neutral and cationic metal–organic complexes for a number of metals (92, 93) coordinated to bulky organic ligands.

Interactions of CO_2 with metal or semiconductor surfaces have been a topic of continued research in the past decades due to the interest in electrochemical conversion of CO_2 into hydrocarbon fuels (3). However, the nature of these interactions is difficult to elucidate in operando due to the complex speciation in the condensed-phase environment of an active electrochemical device. Computational work on the interaction of CO_2 with several different metal surfaces has shown a propensity toward metal–carbon and metal–oxygen interactions straddling neighboring surface atoms prior to CO bond cleavage (137–139).

The formation of two M–O bonds with a single CO_2 ligand in an η^2-(O,O) motif has been identified in several studies involving neutral alkali metal–CO_2 complexes studied by matrix isolation spectroscopy (140–142). These metal carbene species are proposed to be highly reactive, due to the lone pair on the carbon atom. Such a species could be an intermediate state in the formation of C–C bonds. In gas-phase ions, this η^2-(O,O) motif was recently observed by the Uggerud and Asmis groups in $Mg(CO_2)Cl^-$ (143). The infrared signatures of η^2-(O,O) complexes span a wide range (see **Figure 4**) and are less characteristic than those of other ligands discussed here.

There are several other CO_2-containing ligand motifs that involve more than a single CO_2 moiety. One example of more complicated ligand structure is C_2O_4 in various forms (see also Section 4.2). A C_2O_4 ligand can take a planar or a twisted configuration (63), depending on the size of the cation and on whether the metal and the C_2O_4 ligand interact through one or two metal–oxygen bonds. This ligand has been observed in several anionic metal–CO_2 cluster systems, including Bi, Fe, Mn, Ni, and Cu (111, 112, 126, 128, 144). A charge analysis reveals that it has a typical partial charge of about −1.5 e and can therefore be most closely described as oxalate in these cases. Formation of oxalato complexes involving single first-row transition metal centers typically results in planar structures (111, 126, 128, 144). The in-phase combinations of the free CO stretches, along with the in-phase combination of the metal-bound CO stretches, account for the main spectroscopic signatures, occurring in the spectral intervals 1,650–1,700 cm^{-1} and 1,300–1,350 cm^{-1}, respectively. The out-of-phase combinations of these modes usually do not have appreciable infrared activity, distinguishing them from butterfly complexes, where both in-phase and out-of-phase motions can have significant infrared signatures.

Another example of a more complicated CO_2-based ligand is carbonate, where the CO_2 molecule interacts with a metal-oxide species. In the context of the present discussion, it is noteworthy that—apart from genuine metal oxides—the metal oxo functionality can be formed in reactions of metal vapor with CO_2 in a laser vaporization plasma by insertion of a metal atom into a CO bond, resulting in the concomitant formation of a carbonyl ligand (126, 145). Carbonato ligands bind to the metal with one or two metal–oxygen bonds, and such species have been observed in gas-phase $[M(CO_2)_n]^-$ complexes with M = Fe, CoO, and NiO (126, 129). In bidentate η^2-carbonato ligands, two of the CO bonds are strongly influenced by binding to the metal center, resulting in an increase of the CO bond length by ∼12 pm and a decrease of the metal-facing OCO bond angle by ∼10° compared to the 120° in a (hypothetical) free dianion. Work on neutral carbonate-containing complexes of Sc, ScO, and TiO has identified spectral bands that can be assigned to vibrations of the carbonato ligands (146, 147). Typical vibrational signatures of the carbonato ligands can be found at ∼1,600 cm^{-1} (free CO stretch) and ∼1,400 cm^{-1} (metal-bound antisymmetric CO_2 stretch), with a very weak transition occurring at about 1,000 cm^{-1} (totally symmetric CO_3 stretch). Infrared signatures in the range 1,600–1,670 cm^{-1} in spectroelectrochemistry experiments on $[Ni(II)cyclam]^{2+}$ solutions under CO_2 atmosphere at sufficiently negative voltages (<1.2 V) were attributed to bicarbonate ligands coordinated to the Ni(II) center (132).

6. CLOSING REMARKS

Carbon dioxide in intermediate oxidation states is of high importance for CO_2 activation, particularly in the context of CO_2 fixation and solar fuels. Although CO_2 reduction catalysis has been at the center of much work in the past decades, the molecular-level mechanisms involving the different steps in solar fuel catalysis are often poorly understood. In particular, the catalytic cycles themselves, while often built on excellent chemical intuition, need to be confirmed by experiments, and their key intermediate species need to be found and characterized. There are still many open questions in this context, and their answers have direct impact on the validity of models describing the catalytic cycle: What are the active species in molecular CO_2 reduction catalysts (homogeneous or surface immobilized)? What are the active sites in heterogeneous catalyst materials? What is the role of the support for surface-immobilized catalysts? What is the role of the solvent? How does CO_2 bind to the active site?

One of the problems in constructing catalytic cycles and understanding mechanisms is that the analysis of experiments in solution suffers from speciation, particularly under turnover conditions,

where multiple species will be present. As a result, although methods such as infrared spectroelectrochemistry can contain detailed spectroscopic information encoding the nature and state of CO_2 and related species in solution, identification and characterization of reaction intermediates in such systems are very difficult.

An alternative route to the detailed characterization of relevant species is to use mass spectrometric preparation of ionic complexes in tandem with laser spectroscopy, and much of this review has been concerned with the results of such experiments. In the characterization of CO_2 in its many possible roles, such a strategy circumvents many of the complications of speciation in solutions, particularly by employing electrospray ionization to bring the relevant species from solutions into the gas phase. This is a powerful approach, and we can learn about the properties of ionic complexes in vacuo and in clusters in unprecedented detail while maintaining relevant ties to their condensed-phase chemistry. The combination of cryogenic ion traps with electrospray ionization and laser spectroscopy (see, e.g., 148–151 and references therein) has added another set of tools that can now yield spectroscopic information on key species in catalytic cycles (see, e.g., 136) and also prepare solvated metal–organic complexes (152).

Of course, none of these experiments, whether in solution or in vacuo, can be exploited to their full potential without quantum chemical calculations, and conversely, experiments will continue to serve as benchmarks for improving the quality of quantum chemical predictions.

Interleaving these three approaches—spectroelectrochemistry, spectroscopy in vacuo, and quantum chemistry—has the potential to answer the many questions concerning CO_2 activation in the future.

SUMMARY POINTS

1. Negative charge on CO_2 or CO_2-containing functional groups results in lengthening CO bonds and less obtuse OCO bond angles compared to free CO_2, yielding characteristic infrared signatures.
2. The spectral region around 1,600–1,800 cm^{-1} is often highly congested and consistent with many ligand motifs, which can greatly complicate the interpretation of infrared spectra.
3. Clusters and complexes in vacuo, alongside quantum chemical calculations, can serve as model systems to obtain detailed structural information on the interaction of CO_2 with metal centers.

DISCLOSURE STATEMENT

The authors are not aware of any affiliations, memberships, funding, or financial holdings that might be perceived as affecting the objectivity of this review.

ACKNOWLEDGMENTS

We gratefully acknowledge funding from the National Science Foundation (NSF) through the NSF AMO Physics Frontier Center at JILA (PHY-1734006). We also acknowledge graduate student support from the US Department of Education through a GAANN Fellowship for M.C.T. This research was performed while L.G.D. held an NRC Research Associateship award at NIST.

LITERATURE CITED

1. Darwent BdB. 1970. *Bond dissociation energies in simple molecules*. Natl. Stand. Ref. Data Ser., Natl. Bur. Stand. 31, Washington, DC
2. Lias SG. 2017. Ionization energy evaluation. In *NIST Chemistry WebBook, NIST Standard Reference Database 69*, ed. PJ Linstrom, WG Mallard. Gaithersburg, MD: Natl. Inst. Stand. Technol. (NIST)
3. Hori Y. 2008. Electrochemical CO_2 reduction on metal electrodes. In *Modern Aspects of Electrochemistry*, ed. CG Vayenas, RE White, ME Gamboa-Aldeco, pp. 89–189. New York: Springer
4. Lim C-H, Holder AM, Hynes JT, Musgrave CB. 2015. Catalytic reduction of CO_2 by renewable organohydrides. *J. Phys. Chem. Lett.* 6:5078–92
5. Baruch MF, Pander JE, White JL, Bocarsly AB. 2015. Mechanistic insights into the reduction of CO_2 on tin electrodes using in situ ATR-IR spectroscopy. *ACS Catal.* 5:3148–56
6. Appel AM, Bercaw JE, Bocarsly AB, Dobbek H, DuBois DL, et al. 2013. Frontiers, opportunities, and challenges in biochemical and chemical catalysis of CO_2 fixation. *Chem. Rev.* 113:6621–58
7. Van Der Laan GP, Beenackers AACM. 1999. Kinetics and selectivity of the Fischer–Tropsch synthesis: a literature review. *Catal. Rev.* 41:255–318
8. Khadzhiev SN, Kolesnichenko NV, Ezhova NN. 2008. Manufacturing of lower olefins from natural gas through methanol and its derivatives (review). *Petroleum Chem*. 48:325–34
9. Bockris JO, Wass JC. 1989. The photoelectrocatalytic reduction of carbon dioxide. *J. Electrochem. Soc.* 136:2521–28
10. Costentin C, Robert M, Saveant J-M. 2013. Catalysis of the electrochemical reduction of carbon dioxide. *Chem. Soc. Rev.* 42:2423–36
11. Berardi S, Drouet S, Francas L, Gimbert-Surinach C, Guttentag M, et al. 2014. Molecular artificial photosynthesis. *Chem. Soc. Rev.* 43:7501–19
12. Schneider J, Jia H, Muckerman JT, Fujita E. 2012. Thermodynamics and kinetics of CO_2, CO, and H^+ binding to the metal centre of CO_2 reduction catalysts. *Chem. Soc. Rev.* 41:2036–51
13. Kumar B, Llorente M, Froehlich J, Dang T, Sathrum A, Kubiak CP. 2012. Photochemical and photoelectrochemical reduction of CO_2. *Annu. Rev. Phys. Chem.* 63:541–69
14. Kang P, Chen ZF, Brookhart M, Meyer TJ. 2015. Electrocatalytic reduction of carbon dioxide: Let the molecules do the work. *Top. Catal.* 58:30–45
15. Walsh AD. 1953. The electronic orbitals, shapes, and spectra of polyatomic molecules. Part II. Non-hydride AB_2 and BAC molecules. *J. Chem. Soc.* 1953:2266–88
16. Weber JM. 2014. The interaction of negative charge with carbon dioxide—insight into solvation, speciation and reductive activation from cluster studies. *Int. Rev. Phys. Chem.* 33:489–519
17. Sommerfeld T, Meyer HD, Cederbaum LS. 2004. Potential energy surface of the CO_2^- anion. *Phys. Chem. Chem. Phys.* 6:42–45
18. Ovenall DW, Whiffen DH. 1961. Electron spin resonance and structure of the CO_2^- radical ion. *Mol. Phys.* 4:135–44
19. Compton RN, Reinhardt PW, Cooper CD. 1975. Collisional ionization of Na, K, and Cs by CO_2, COS, and Cs_2—molecular electron affinities. *J. Chem. Phys.* 63:3821–27
20. Gutsev GL, Bartlett RJ, Compton RN. 1998. Electron affinities of CO_2, OCS, and CS_2. *J. Chem. Phys.* 108:6756–62
21. Arnold ST, Coe JV, Eaton JG, Freidhoff CB, Kidder LH, et al. 1990. Photodetachment spectroscopy of negative cluster ions. In *The Chemical Physics of Atomic and Molecular Clusters: Varenna on Lake Como, Villa Monastero, June 28–July 7, 1988*, ed. G Scoles, pp. 467–90. New York: Elsevier
22. Knapp M, Echt O, Kreisle D, Märk TD, Recknagel E. 1986. Formation of long-lived CO_2^-, N_2O^-, and their dimer anions, by electron-attachment to Van-der-Waals clusters. *Chem. Phys. Lett.* 126:225–31
23. Raarup MK, Andersen HH, Andersen T. 1999. Metastable state of CO_2^- with millisecond lifetime. *J. Phys. B* 32:L659–64
24. Schröder D, Schalley CA, Harvey JN, Schwarz H. 1999. On the formation of the carbon dioxide anion radical $CO_2^{-\bullet}$ in the gas phase. *Int. J. Mass Spectrom.* 187:25–35
25. Jacox ME, Milligan DE. 1974. Vibrational spectrum of CO_2^- in an argon matrix. *Chem. Phys. Lett.* 28:163–68

26. Thompson WE, Jacox ME. 1999. The vibrational spectra of CO_2^+, $(CO_2)_2^+$, CO_2^-, and $(CO_2)_2^-$ trapped in solid neon. *J. Chem. Phys.* 111:4487–96
27. Zhou M, Andrews L. 1999. Infrared spectra of the CO_2^- and $C_2O_4^-$ anions isolated in solid argon. *J. Chem. Phys.* 110:2414–22
28. Takahashi K, Sawamura S, Dimitrijevic NM, Bartels DM, Jonah CD. 2002. Transient negative species in supercritical carbon dioxide: electronic spectra and reactions of CO_2 anion clusters. *J. Phys. Chem. A* 106:108–14
29. Shkrob IA, Sauer MC. 2001. Metastable electrons, high-mobility solvent anions, and charge transfer reactions in supercritical carbon dioxide. *J. Phys. Chem. B* 105:4520–30
30. Janik I, Tripathi GNR. 2016. The nature of the CO_2^- radical anion in water. *J. Chem. Phys.* 144:154307
31. DeLuca MJ, Niu B, Johnson MA. 1988. Photoelectron spectroscopy of $(CO_2)_2^-$ clusters with $2 \le n \le 13$: cluster size dependence of the core molecular ion. *J. Chem. Phys.* 88:5857–63
32. Tsukuda T, Johnson MA, Nagata T. 1997. Photoelectron spectroscopy of $(CO_2)_n^-$ revisited: core switching in the $2 \le n \le 16$ range. *Chem. Phys. Lett.* 268:429–33
33. Shin JW, Hammer NI, Johnson MA, Schneider H, Glöss A, Weber JM. 2005. An infrared investigation of the $(CO_2)_n^-$ clusters: core ion switching from both the ion and solvent perspectives. *J. Phys. Chem. A* 109:3146–52
34. Shimanouchi T. 1972. *Tables of molecular vibrational frequencies, consolidated volume I*. Natl. Stand. Ref. Data Ser., Natl. Bur. Stand. 39, Washington, DC
35. DePalma JW, Kelleher PJ, Tavares LC, Johnson MA. 2017. Coordination-dependent spectroscopic signatures of divalent metal ion binding to carboxylate head groups: H_2- and He-tagged vibrational spectra of $M^{2+} \bullet RCO_2^-$ (M = Mg and Ca, R = $-CD_3$, $-CD_2CD_3$) complexes. *J. Phys. Chem. Lett.* 8:484–88
36. Dodson LG, Thompson MC, Weber JM. 2017. Unpublished research
37. Chantry GW, Whiffen DH. 1962. Electronic absorption spectra of CO_2^- trapped in γ-irradiated crystalline sodium formate. *Mol. Phys.* 5:189–94
38. Velarde L, Habteyes T, Sanov A. 2006. Photodetachment and photofragmentation pathways in the $[(CO_2)_2(H_2O)_m]^-$ cluster anions. *J. Chem. Phys.* 125:114303
39. Habteyes T, Velarde L, Sanov A. 2007. Photodissociation of CO_2^- in water clusters via Renner–Teller and conical interactions. *J. Chem. Phys.* 126:154301
40. Habteyes T, Velarde L, Sanov A. 2006. Solvent-enabled photodissociation of CO_2^- in water clusters. *Chem. Phys. Lett.* 424:268–72
41. Jacox ME. 2017. Vibrational and electronic energy levels of polyatomic transient molecules. In *NIST Chemistry WebBook, NIST Standard Reference Database*, ed. PJ Linstrom, WG Mallard. Gaithersburg, MD: Natl. Inst. Stand. Technol. (NIST)
42. Kawaguchi K, Yamada C, Hirota E. 1985. Diode laser spectroscopy of the CO_2^+ ν_3 band using magnetic field modulation of the discharge plasma. *J. Chem. Phys.* 82:1174–77
43. Inokuchi Y, Kobayashi Y, Muraoka A, Nagata T, Ebata T. 2009. Structures of water–CO_2 and methanol–CO_2 cluster ions: $[H_2O \bullet (CO_2)_n]^+$ and $[CH_3OH \bullet (CO_2)_n]^+$ ($n = 1$–7). *J. Chem. Phys.* 130:154304
44. Mabbs R, Surber E, Velarde L, Sanov A. 2004. Effects of solvation and core switching on the photoelectron angular distributions from $(CO_2)_n^-$ and $(CO_2)_n^- \bullet H_2O$. *J. Chem. Phys.* 120:5148–54
45. Sommerfeld T, Posset T. 2003. Electron attachment to CO_2 clusters. *J. Chem. Phys.* 119:7714–24
46. Zhou M, Andrews L. 1999. Infrared spectra of the $C_2O_4^+$ cation and $C_2O_4^-$ anion isolated in solid neon. *J. Chem. Phys.* 110:6820–26
47. Kamrath MZ, Relph RA, Johnson MA. 2010. Vibrational predissociation spectrum of the carbamate radical anion, $C_5H_5N\text{-}CO_2^-$, generated by reaction of pyridine with $(CO_2)_m^-$. *J. Am. Chem. Soc.* 132:15508–11
48. Ricks AM, Brathwaite AD, Duncan MA. 2013. IR spectroscopy of gas phase $V(CO_2)_n^+$ clusters: solvation-induced electron transfer and activation of CO_2. *J. Phys. Chem. A* 117:11490–98
49. Muraoka A, Inokuchi Y, Nishi N, Nagata T. 2005. Structures of $[(CO_2)_n(H_2O)_m]^-$ ($n = 1$–4, $m = 1,2$) cluster anions. I. Infrared photodissociation spectroscopy. *J. Chem. Phys.* 122:094303

50. Kondo M, Takayanagi T. 2017. The effects of water microsolvation on the $C_2O_4^- \leftrightarrow CO_2 \bullet CO_2^-$ core switching reaction: perspective from exploration of pathways on the potential energy surfaces of small $[(CO_2)_2(H_2O)_n]^-$ ($n = 1$ and 2) clusters. *Comput. Theor. Chem.* 1105:61–68
51. Muraoka A, Inokuchi Y, Nagata T. 2008. Structures of $[(CO_2)_n(CH_3OH)_m]^-$ ($n = 1$–4, $m = 1, 2$) cluster anions. *J. Phys. Chem. A* 112:4906–13
52. Thompson MC, Weber JM. 2017. Enhancement of infrared activity by moving electrons through bonds—the case of CO_2 anion and carboxylate. *Chem. Phys. Lett.* 683:586–90
53. Kim EH, Bradforth SE, Arnold DW, Metz RB, Neumark DM. 1995. Study of HCO_2 and DCO_2 by negative ion photoelectron spectroscopy. *J. Chem. Phys.* 103:7801–14
54. Krekeler C, Mladenovic M, Botschwina P. 2005. A theoretical investigation of the vibrational states of HCO_2^- and its isotopomers. *Phys. Chem. Chem. Phys.* 7:882–87
55. Gerardi HK, DeBlase AF, Su X, Jordan KD, McCoy AB, Johnson MA. 2011. Unraveling the anomalous solvatochromic response of the formate ion vibrational spectrum: an infrared, Ar-tagging study of the HCO_2^-, DCO_2^-, and $HCO_2^- \bullet H_2O$ ions. *J. Phys. Chem. Lett.* 2:2437–41
56. Forney D, Jacox ME, Thompson WE. 2003. Infrared spectra of *trans*-HOCO, $HCOOH^+$, and HCO_2^- trapped in solid neon. *J. Chem. Phys.* 119:10814–23
57. Kidd KG, Mantsch HH. 1981. Formate anion: the physical force field. *J. Mol. Spectrosc.* 85:375–89
58. Bartholomew RJ, Irish DE. 1993. Raman spectral studies of solutions at elevated temperatures and pressures. 13. Sodium formate–water. *Can. J. Chem.* 71:1728–33
59. Gennaro A, Isse AA, Severin M-G, Vianello E, Bhugun I, Saveant J-M. 1996. Mechanism of the electrochemical reduction of carbon dioxide at inert electrodes in media of low proton availability. *J. Chem. Soc. Faraday Trans.* 92:3963–68
60. Herbert JM, Ortiz JV. 2000. Ab initio investigation of electron detachment in dicarboxylate dianions. *J. Phys. Chem. A* 104:11786–95
61. Wang X-B, Yang X, Nicholas JB, Wang L-S. 2003. Photodetachment of hydrated oxalate dianions in the gas phase, $C_2O_4^{2-}(H_2O)_n$ ($n = 3$–40): from solvated clusters to nanodroplet. *J. Chem. Phys.* 119:3631–40
62. Gao B, Liu Z-f. 2005. First principles study on the solvation and structure of $C_2O_4^{2-}(H_2O)_n$, $n = 6$–12. *J. Phys. Chem. A* 109:9104–11
63. Dean PAW. 2012. The oxalate dianion, $C_2O_4^{2-}$: planar or nonplanar? *J. Chem. Educ.* 89:417–18
64. Rosas-García VM, del Carmen Sáenz-Tavera I, Rodríguez-Herrera VJ, Garza-Campos BR. 2013. Microsolvation and hydration enthalpies of $CaC_2O_4(H_2O)_n$ ($n = 0$–16) and $C_2O_4^{2-}(H_2O)_n$ ($n = 0$–14): an *ab initio* study. *J. Mol. Model.* 19:1459–71
65. Kroutil O, Minofar B, Kabeláč M. 2016. Structure and dynamics of solvated hydrogenoxalate and oxalate anions: a theoretical study. *J. Mol. Model.* 22:210
66. Wang X-B, Yang X, Nicholas JB, Wang L-S. 2001. Bulk-like features in the photoemission spectra of hydrated doubly charged anion clusters. *Science* 294:1322–25
67. Pathak AK. 2014. Conductance and bulk vertical detachment energy of hydrated sulphate and oxalate dianions: a theoretical study. *Mol. Phys.* 112:1548–52
68. Delahay P. 1982. Photoelectron emission spectroscopy of aqueous solutions. *Acc. Chem. Res.* 15:40–45
69. Begun GM, Fletcher WH. 1963. Vibrational spectra of aqueous oxalate ion. *Spectrochim. Acta* 19:1343–49
70. Clark RJH, Firth S. 2002. Raman, infrared and force field studies of $K_2{}^{12}C_2O_4 \bullet H_2O$ and $K_2{}^{13}C_2O_4 \bullet H_2O$ in the solid state and in aqueous solution, and of $(NH_4)_2{}^{12}C_2O_4 \bullet H_2O$ and $(NH_4)_2{}^{13}C_2O_4 \bullet H_2O$ in the solid state. *Spectrochim. Acta A* 58:1731–46
71. Peterson KI, Pullman DP. 2016. Determining the structure of oxalate anion using infrared and Raman spectroscopy coupled with Gaussian calculations. *J. Chem. Educ.* 93:1130–33
72. Kuroda DG, Hochstrasser RM. 2011. Two-dimensional infrared spectral signature and hydration of the oxalate dianion. *J. Chem. Phys.* 135:204502
73. Wolke CT, DeBlase AF, Leavitt CM, McCoy AB, Johnson MA. 2015. Diffuse vibrational signature of a single proton embedded in the oxalate scaffold, $HO_2CCO_2^-$. *J. Phys. Chem. A* 119:13018–24
74. Loerting T, Bernard J. 2010. Aqueous carbonic acid (H_2CO_3). *Chem. Phys. Chem.* 11:2305–9
75. Reddy SK, Balasubramanian S. 2014. Carbonic acid: molecule, crystal and aqueous solution. *Chem. Commun.* 50:503–14

76. Rudolph WW, Irmer G, Konigsberger E. 2008. Speciation studies in aqueous HCO_3^-–CO_3^{2-} solutions. A combined Raman spectroscopic and thermodynamic study. *Dalton Trans.* 900–8
77. Janoschek R. 1992. Are the 'textbook anions' O^{2-}, $[CO_3]^{2-}$, and $[SO_4]^{2-}$ fictitious? *Z. Anorg. Allg. Chem.* 616:101–4
78. Boldyrev AI, Gutowski M, Simons J. 1996. Small multiply charged anions as building blocks in chemistry. *Acc. Chem. Res.* 29:497–502
79. Sommerfeld T. 2000. Lifetimes of metastable dianions: CN_2^{2-}, C_4^{2-}, and CO_3^{2-}. *J. Phys. Chem. A* 104:8806–13
80. Davis AR, Oliver BG. 1972. A vibrational-spectroscopic study of the species present in the CO_2–H_2O system. *J. Solution Chem.* 1:329–39
81. Oliver BG, Davis AR. 1973. Vibrational spectroscopic studies of aqueous alkali metal bicarbonate and carbonate solutions. *Can. J. Chem.* 51:698–702
82. Iwasita T, Nart FC, Rodes A, Pastor E, Weber M. 1995. Vibrational spectroscopy at the electrochemical interface. *Electrochim. Acta* 40:53–59
83. Sipos P, Bolden L, Hefter G, May PM. 2000. Raman spectroscopic study of ion pairing of alkali metal ions with carbonate and sulfate in aqueous solutions. *Aust. J. Chem.* 53:887–90
84. Sun Q, Qin C. 2011. Raman OH stretching band of water as an internal standard to determine carbonate concentrations. *Chem. Geol.* 283:274–78
85. Dobson KD, McQuillan AJ. 1997. An infrared spectroscopic study of carbonate adsorption to zirconium dioxide sol-gel films from aqueous solutions. *Langmuir* 13:3392–96
86. Rudolph WW, Fischer D, Irmer G. 2006. Vibrational spectroscopic studies and density functional theory calculations of speciation in the CO_2–water system. *Appl. Spectrosc.* 60:130–44
87. Goldsmith JA, Ross SD. 1968. Factors affecting the infra-red spectra of planar anions with D_{3h} symmetry—IV. The vibrational spectra of some complex carbonates in the region 4,000–400 cm^{-1}. *Spectrochim. Acta A* 24:993–98
88. Lee H, Wilmshurst J. 1964. Observation of ion-pairs in aqueous solutions by vibrational spectroscopy. *Aust. J. Chem.* 17:943–45
89. Iwasita T, Rodes A, Pastor E. 1995. Vibrational spectroscopy of carbonate adsorbed on Pt(111) and Pt(110) single-crystal electrodes. *J. Electroanal. Chem.* 383:181–89
90. Pezzotti G, Puppulin L, La Rosa A, Boffelli M, Zhu W, et al. 2015. Effect of pH and monovalent cations on the Raman spectrum of water: basics revisited and application to measure concentration gradients at water/solid interface in Si_3N_4 biomaterial. *Chem. Phys.* 463:120–36
91. Garand E, Wende T, Goebbert DJ, Bergmann R, Meijer G, et al. 2010. Infrared spectroscopy of hydrated bicarbonate anion clusters: $HCO_3^-(H_2O)_{1-10}$. *J. Am. Chem. Soc.* 132:849–56
92. Gibson DH. 1999. Carbon dioxide coordination chemistry: metal complexes and surface-bound species. What relationships? *Coord. Chem. Rev.* 185–86:335–55
93. Gibson DH. 1996. The organometallic chemistry of carbon dioxide. *Chem. Rev.* 96:2063–96
94. Armentrout PB. 2001. Reactions and thermochemistry of small transition metal cluster ions. *Annu. Rev. Phys. Chem.* 52:423–61
95. Schwarz H. 2017. Metal-mediated activation of carbon dioxide in the gas phase: mechanistic insight derived from a combined experimental/computational approach. *Coord. Chem. Rev.* 334:112–23
96. Jaeger JB, Jaeger TD, Brinkmann NR, Schaefer HF, Duncan MA. 2004. Infrared photodissociation spectroscopy of $Si^+(CO_2)_n$ and $Si^+(CO_2)_nAr$ complexes—evidence for unanticipated intracluster reactions. *Can. J. Chem.* 82:934–46
97. Walker NR, Walters RS, Grieves GA, Duncan MA. 2004. Growth dynamics and intracluster reactions in $Ni^+(CO_2)_n$ complexes via infrared spectroscopy. *J. Chem. Phys.* 121:10498–507
98. Walker NR, Walters RS, Duncan MA. 2004. Infrared photodissociation spectroscopy of $V^+(CO_2)_n$ and $V^+(CO_2)_nAr$ complexes. *J. Chem. Phys.* 120:10037–45
99. Gregoire G, Velasquez J, Duncan MA. 2001. Infrared photodissociation spectroscopy of small $Fe^+(CO_2)_n$ and $Fe^+(CO_2)_n$ Ar clusters. *Chem. Phys. Lett.* 349:451–57
100. Gregoire G, Duncan MA. 2002. Infrared spectroscopy to probe structure and growth dynamics in Fe^+-$(CO_2)_n$ clusters. *J. Chem. Phys.* 117:2120–30

101. Walters RS, Brinkmann NR, Schaefer HF, Duncan MA. 2003. Infrared photodissociation spectroscopy of mass-selected $Al^+(CO_2)_n$ and $Al^+(CO_2)_nAr$ clusters. *J. Phys. Chem. A* 107:7396–405
102. Scurlock CT, Pullins SH, Duncan MA. 1996. Photodissociation spectroscopy of Ca^+CO_2. *J. Chem. Phys.* 105:3579–85
103. Iskra A, Gentleman AS, Kartouzian A, Kent MJ, Sharp AP, Mackenzie SR. 2017. Infrared spectroscopy of gas-phase $M^+(CO_2)_n$ (M = Co, Rh, Ir) ion–molecule complexes. *J. Phys. Chem. A* 121:133–40
104. Xu S, Smith JET, Weber JM. 2016. Ligand influence on the electronic spectra of dicationic ruthenium-bipyridine-terpyridine complexes. *J. Phys. Chem. A* 120:2350–56
105. Heiz U, Bullock EL. 2004. Fundamental aspects of catalysis on supported metal clusters. *J. Mater. Chem.* 14:564–77
106. Haruta M. 1997. Size- and support-dependency in the catalysis of gold. *Catal. Today* 36:153–66
107. Haruta M. 2005. Catalysis: gold rush. *Nature* 437:1098–99
108. Haruta M, Date M. 2001. Advances in the catalysis of Au nanoparticles. *Appl. Catal. A* 222:427–37
109. Knurr BJ, Weber JM. 2012. Solvent-driven reductive activation of carbon dioxide by gold anions. *J. Am. Chem. Soc.* 134:18804–8
110. Knurr BJ, Weber JM. 2013. Solvent-mediated reduction of carbon dioxide in anionic complexes with silver atoms. *J. Phys. Chem. A* 117:10764–71
111. Knurr BJ, Weber JM. 2014. Structural diversity of copper–CO_2 complexes: infrared spectra and structures of $[Cu(CO_2)_n]^-$ clusters. *J. Phys. Chem. A* 118:10246–51
112. Thompson MC, Ramsay J, Weber JM. 2016. Solvent-driven reductive activation of CO_2 by bismuth: switching from metalloformate complexes to oxalate products. *Angew. Chem. Int. Ed.* 55:15171–74
113. Arnold DW, Bradforth SE, Kim EH, Neumark DM. 1995. Study of $I^-(CO_2)_n$, $Br^-(CO_2)_n$, and $I^-(N_2O)_n$ clusters by anion photoelectron spectroscopy. *J. Chem. Phys.* 102:3510–18
114. Markovich G, Giniger R, Levin M, Cheshnovsky O. 1991. Photoelectron spectroscopy of negative ions solvated in clusters. *Z. Phys. D* 20:69–72
115. Weber JM, Schneider H. 2004. Infrared spectra of $X^- \cdot CO_2 \cdot Ar$ cluster anions (X = Cl, Br, I). *J. Chem. Phys.* 120:10056–61
116. Mbaiwa F, Dao D, Holtgrewe N, Lasinski J, Mabbs R. 2012. Inter-channel effects in monosolvated atomic iodide cluster anion detachment: correlation of the anisotropy parameter with solvent dipole moment. *J. Chem. Phys.* 136:114303
117. Calabrese JC, Herskovitz T, Kinney JB. 1983. Carbon dioxide coordination chemistry. 5. The preparation and structure of the rhodium complex $Rh(\eta^1\text{-}CO_2)(Cl)(diars)_2$. *J. Am. Chem. Soc.* 105:5914–15
118. Harlow RL, Kinney JB, Herskovitz T. 1980. Carbon dioxide co-ordination chemistry: preparation and X-ray crystal structure of the methoxycarbonyl complex $[IrCl(CO_2Me)\text{-}(Me_2PCH_2CH_2PMe_2)_2]FSO$ from a CO adduct. *J. Chem. Soc. Chem. Commun.* 1980(17):813–14
119. Tanaka K, Ooyama D. 2002. Multi-electron reduction of CO_2 via Ru-CO_2, -C(O)OH, -CO, -CHO, and -CH_2OH species. *Coord. Chem. Rev.* 226:211–18
120. Riplinger C, Sampson MD, Ritzmann AM, Kubiak CP, Carter EA. 2014. Mechanistic contrasts between manganese and rhenium bipyridine electrocatalysts for the reduction of carbon dioxide. *J. Am. Chem. Soc.* 136:16285–98
121. Guo Z, Cheng S, Cometto C, Anxolabéhère-Mallart E, Ng S-M, et al. 2016. Highly efficient and selective photocatalytic CO_2 reduction by iron and cobalt quaterpyridine complexes. *J. Am. Chem. Soc.* 138:9413–16
122. Leung K, Nielsen IMB, Sai N, Medforth C, Shelnutt JA. 2010. Cobalt-porphyrin catalyzed electrochemical reduction of carbon dioxide in water. 2. Mechanism from first principles. *J. Phys. Chem. A* 114:10174–84
123. Fujita E, Creutz C, Sutin N, Brunschwig BS. 1993. Carbon dioxide activation by cobalt macrocycles: evidence of hydrogen bonding between bound CO_2 and the macrocycle in solution. *Inorg. Chem.* 32:2657–62
124. Bhugun I, Lexa D, Saveant JM. 1996. Catalysis of the electrochemical reduction of carbon dioxide by iron(0) porphyrins: synergystic effect of weak Bronsted acids. *J. Am. Chem. Soc.* 118:1769–76
125. Song J, Klein EL, Neese F, Ye S. 2014. The mechanism of homogeneous CO_2 reduction by Ni(cyclam): product selectivity, concerted proton–electron transfer and C–O bond cleavage. *Inorg. Chem.* 53:7500–7

126. Thompson MC, Dodson LG, Weber JM. 2017. Structural motifs of $[Fe(CO_2)_n]^-$ clusters ($n = 3–7$). *J. Phys. Chem. A* 121:4132–38
127. Knurr BJ, Weber JM. 2014. Infrared spectra and structures of anionic complexes of cobalt with carbon dioxide ligands. *J. Phys. Chem. A* 118:4056–62
128. Knurr BJ, Weber JM. 2014. Interaction of nickel with carbon dioxide in $[Ni(CO_2)_n]^-$ clusters studied by infrared spectroscopy. *J. Phys. Chem. A* 118:8753–57
129. Knurr BJ, Weber JM. 2015. Structures of $[CoO(CO_2)_n]^-$ and $[NiO(CO_2)_n]^-$ clusters studied by infrared spectroscopy. *J. Phys. Chem. A* 119:843–50
130. Hossain E, Rothgeb DW, Jarrold CC. 2010. CO_2 reduction by group 6 transition metal suboxide cluster anions. *J. Chem. Phys.* 133:024305
131. Rothgeb DW, Hossain E, Mann JE, Jarrold CC. 2010. Disparate product distributions observed in $Mo_{(3-x)}W_xO_y^-$ ($x = 0–3$; $y = 3–9$) reactions with D_2O and CO_2. *J. Chem. Phys.* 132:064302
132. Froehlich JD, Kubiak CP. 2012. The homogeneous reduction of CO_2 by $[Ni(cyclam)]^+$: increased catalytic rates with the addition of a CO scavenger. *J. Am. Chem. Soc.* 137:3565–73
133. Beley M, Collin JP, Ruppert R, Sauvage JP. 1986. Electrocatalytic reduction of carbon dioxide by nickel $cyclam^{2+}$ in water: study of the factors affecting the efficiency and the selectivity of the process. *J. Am. Chem. Soc.* 108:7461–67
134. Neri G, Aldous IM, Walsh JJ, Hardwick LJ, Cowan AJ. 2016. A highly active nickel electrocatalyst shows excellent selectivity for CO_2 reduction in acidic media. *Chem. Sci.* 7:1521–26
135. Hammouche M, Lexa D, Momenteau M, Saveant JM. 1991. Chemical catalysis of electrochemical reactions. Homogeneous catalysis of the electrochemical reduction of carbon dioxide by iron("0") porphyrins. Role of the addition of magnesium cations. *J. Am. Chem. Soc.* 113:8455–66
136. Menges FS, Craig SM, Tötsch N, Bloomfield A, Ghosh S, et al. 2016. Capture of CO_2 by a cationic nickel(I) complex in the gas phase and characterization of the bound, activated CO_2 molecule by cryogenic ion vibrational predissociation spectroscopy. *Angew. Chem. Int. Ed.* 55:1282–85
137. Liu C, Cundari TR, Wilson AK. 2012. CO_2 reduction on transition metal (Fe, Co, Ni, and Cu) surfaces: in comparison with homogeneous catalysis. *J. Phys. Chem. C* 116:5681–88
138. Sheng T, Sun SG. 2017. Electrochemical reduction of CO_2 into CO on Cu(100): a new insight into the C–O bond breaking mechanism. *Chem. Commun.* 53:2594–97
139. Wu HW, Zhang N, Cao ZJ, Wang HM, Hong SU. 2012. The adsorption of CO_2, H_2CO_3, HCO_3^- and CO_3^{2-} on $Cu_2O(111)$ surface: first-principles study. *Int. J. Quantum Chem.* 112:2532–40
140. Kafafi ZH, Hauge RH, Billups WE, Margrave JL. 1984. Carbon dioxide activation by alkali metals. 2. Infrared spectra of $M^+CO_2^-$ and $M_2^{2+}CO_2^{2-}$ in argon and nitrogen matrixes. *Inorg. Chem.* 23:177–83
141. Manceron L, Loutellier A, Perchard JP. 1985. Reduction of carbon dioxide to oxalate by lithium atoms: a matrix isolation study of the intermediate steps. *J. Mol. Struct.* 129:115–24
142. Solov'ev VN, Polikarpov EV, Nemukhin AV, Sergeev GB. 1999. Matrix isolation and ab initio study of the reactions of magnesium atoms and clusters with CO_2, C_2H_4, and CO_2/C_2H_4 mixtures: formation of cyclic complexes. *J. Phys. Chem. A* 103:6721–25
143. Miller GBS, Esser TK, Knorke H, Gewinner S, Schöllkopf W, et al. 2014. Spectroscopic identification of a bidentate binding motif in the anionic magnesium–CO_2 complex ($[ClMgCO_2]^-$). *Angew. Chem. Int. Ed.* 53:14407–10
144. Thompson MC, Ramsay J, Weber JM. 2017. Interaction of CO_2 with atomic manganese in the presence of an excess negative charge probed by infrared spectroscopy of $[Mn(CO_2)_n]^-$ clusters. *J. Phys. Chem. A* 121:7534–42
145. Yanagimachi A, Koyasu K, Valdivielso DY, Gewinner S, Schöllkopf W, et al. 2016. Size-specific, dissociative activation of carbon dioxide by cobalt cluster anions. *J. Phys. Chem. C* 120:14209–15
146. Zhang Q, Qu H, Chen M, Zhou M. 2016. Carbon dioxide activation by scandium atoms and scandium monoxide molecules: formation and spectroscopic characterization of $ScCO_3$ and $OCScCO_3$ in solid neon. *J. Phys. Chem. A* 120:425–32
147. Zhuang J, Li ZH, Fan K, Zhou M. 2012. Matrix isolation spectroscopic and theoretical study of carbon dioxide activation by titanium oxide molecules. *J. Phys. Chem. A* 116:3388–95
148. Wang XB, Yang X, Wang LS. 2002. Probing solution-phase species and chemistry in the gas phase. *Int. Rev. Phys. Chem.* 21:473–98

149. Wang XB, Wang LS. 2008. Development of a low-temperature photoelectron spectroscopy instrument using an electrospray ion source and a cryogenically controlled ion trap. *Rev. Sci. Instrum.* 79:073108
150. Rizzo TR, Boyarkin OV. 2015. Cryogenic methods for the spectroscopy of large, biomolecular ions. In *Gas-Phase IR Spectroscopy and Structure of Biological Molecules*, ed. AM Rijs, J Oomens, pp. 43–97. Cham, Switz.: Springer
151. Wolk AB, Leavitt CM, Garand E, Johnson MA. 2014. Cryogenic ion chemistry and spectroscopy. *Acc. Chem. Res.* 47:202–10
152. Marsh BM, Voss JM, Garand E. 2015. A dual cryogenic ion trap spectrometer for the formation and characterization of solvated ionic clusters. *J. Chem. Phys.* 143:204201

Annual Review of
Physical Chemistry
Volume 69, 2018

Contents

Indexes

Errata

An online log of corrections to *Annual Review of Physical Chemistry* articles may be found at http://www.annualreviews.org/errata/physchem